



Identification of sulphonamide-tethered *N*-((triazol-4-yl)methyl)isatin derivatives as inhibitors of SARS-CoV-2 main protease

Mai H. ElNaggar, Abdullah A. Elgazar, Ghada Gamal, Shimaa M. Hamed, Zainab M. Elsayed, Mohamed K. El-Ashrey, Amira Abood, Mahmoud A. El Hassab, Ahmed M. Soliman, Ramadan A. El-Domany, Farid A. Badria, Claudiu T. Supuran & Wagdy M. Eldehna

To cite this article: Mai H. ElNaggar, Abdullah A. Elgazar, Ghada Gamal, Shimaa M. Hamed, Zainab M. Elsayed, Mohamed K. El-Ashrey, Amira Abood, Mahmoud A. El Hassab, Ahmed M. Soliman, Ramadan A. El-Domany, Farid A. Badria, Claudiu T. Supuran & Wagdy M. Eldehna (2023) Identification of sulphonamide-tethered *N*-((triazol-4-yl)methyl)isatin derivatives as inhibitors of SARS-CoV-2 main protease, *Journal of Enzyme Inhibition and Medicinal Chemistry*, 38:1, 2234665, DOI: [10.1080/14756366.2023.2234665](https://doi.org/10.1080/14756366.2023.2234665)

To link to this article: <https://doi.org/10.1080/14756366.2023.2234665>



© 2023 The Author(s). Published by Informa UK Limited, trading as Taylor & Francis Group.



[View supplementary material](#)



Published online: 11 Jul 2023.



[Submit your article to this journal](#)



Article views: 374



[View related articles](#)







[View Crossmark data](#)

RESEARCH ARTICLE



Identification of sulphonamide-tethered *N*-((triazol-4-yl)methyl)isatin derivatives as inhibitors of SARS-CoV-2 main protease

Mai H. ElNaggar^a , Abdullah A. Elgazar^a , Ghada Gamal^a, Shimaa M. Hamed^b, Zainab M. Elsayed^b, Mohamed K. El-Ashrey^c, Amira Abood^{d,e}, Mahmoud A. El Hassab^f, Ahmed M. Soliman^g, Ramadan A. El-Domany^g, Farid A. Badria^h, Claudiu T. Supuranⁱ  and Wagdy M. Eldehna^{j,k} 

^aDepartment of Pharmacognosy, Faculty of Pharmacy, Kafrelsheikh University, Kafrelsheikh, Egypt; ^bScientific Research and Innovation Support Unit, Faculty of Pharmacy, Kafrelsheikh University, Kafrelsheikh, Egypt; ^cPharmaceutical Chemistry Department, Faculty of Pharmacy, Cairo University, Cairo, Egypt; ^dChemistry of Natural and microbial products, National Research center, Egypt; ^eDepartment of Bioscience, University of Kent, Canterbury, UK; ^fDepartment of Medicinal Chemistry, Faculty of Pharmacy, King Salman International University (KSIU), Egypt; ^gDepartment of Microbiology and Immunology, Faculty of Pharmacy, Kafrelsheikh University, Kafrelsheikh, Egypt; ^hDepartment of Pharmacognosy, Faculty of Pharmacy, Mansoura University, Mansoura, Egypt; ⁱDepartment of NEUROFARBA, Section of Pharmaceutical and Nutraceutical Sciences, University of Florence, Firenze, Italy; ^jDepartment of Pharmaceutical Chemistry, Faculty of Pharmacy, Kafrelsheikh University, Kafrelsheikh, Egypt; ^kSchool of Biotechnology, Badr University in Cairo, Badr City, Egypt

ABSTRACT

SARS-CoV-2 pandemic in the end of 2019 led to profound consequences on global health and economy. Till producing successful vaccination strategies, the healthcare sectors suffered from the lack of effective therapeutic agents that could control the spread of infection. Thus, academia and the pharmaceutical sector prioritise SARS-CoV-2 antiviral drug discovery. Here, we exploited previous reports highlighting the anti-SARS-CoV-2 activities of isatin-based molecules to develop novel triazolo-isatins for inhibiting main protease (Mpro) of the virus, a crucial enzyme for its replication in the host cells. Particularly, sulphonamide **6b** showed promising inhibitory activity with an $IC_{50} = 0.249 \mu M$. Additionally, **6b** inhibited viral cell proliferation with an IC_{50} of $4.33 \mu g/ml$, and was non-toxic to VERO-E6 cells ($CC_{50} = 564.74 \mu g/ml$) displaying a selectivity index of 130.4. *In silico* analysis of **6b** disclosed its ability to interact with key residues in the enzyme active site, supporting the obtained *in vitro* findings.

ARTICLE HISTORY

Received 20 April 2023
Revised 9 June 2023
Accepted 3 July 2023

KEYWORDS

Isatin derivatives; click chemistry; SARS-CoV-2; main protease; FRET assay and molecular docking




Introduction


Since the World Health Organisation (WHO) declared COVID-19 a pandemic in 2019, the rapid spread of SARS-CoV-2 has resulted in more than 620 million confirmed cases and the deaths of millions of people¹, making it one of the most catastrophic global health disasters in human history². There are now only a few SARS-CoV-2 medicines available, despite the widespread approval of vaccination^{3,4}. In addition to this, the emergence of SARS-CoV-2 omicron subvariants that are effective poses a threat to the efficacy of vaccines developed for the purpose of controlling COVID-19 infection^{5,6}. Hence, the search for effective therapeutic drugs to combat SARS-CoV-2 is urgently needed.

In the search for inhibitors of SARS-CoV-2, several viral targets that are essential to the replication of the virus are being investigated. One of these viral targets is the SARS-CoV-2 main protease (Mpro)⁷. The 1a/1ab polyprotein (pp), which is the target of Mpro's proteolytic activity⁸, is hydrolysed into 16 mature non-structural proteins (NSPs)⁹. These proteins play crucial roles in the initial stages of the SARS-CoV-2 replication cycle, including the synthesis of RNA of the virus, the rearrangement for the host cell cytoplasmic organelles to create environments favourable for viral

replication, the production of structural, and construction of new viral particles which eventually would be released to other host cells. The Protomers A and B constitute the homodimer protease which are responsible for the catalytic function of enzyme through thiol group of Cys145 and deprotonated His41 which is considered as the catalytic dyad of Mpro¹⁰. Hence, the disruption of the catalytic activity of Mpro may therefore be a useful and promising strategy, as demonstrated by the clinical success of nirmatrelvir, the first Mpro inhibitor to enter into clinical use¹¹.

There are two categories of SARS-CoV-2 Mpro inhibitors, non-covalent inhibitors like X77 and ML188 or covalent inhibitors (such as N3 and GC376)¹². The covalent inhibitor forms a covalent bond with catalytic dyad, which blocks the binding site. On the other hand, non-covalent inhibitor does not require covalent binding to block the Mpro enzyme⁷. Despite the advantages of covalent inhibitors and their current resurrection, concerns about their safety, such as the possibility of off-target effects and delayed effects, have always hampered the development of such new medications, although, as mentioned above, nirmatrelvir constitutes an exception^{13–14}.

CONTACT Mai H. ElNaggar  mai_elnaggar@pharm.kfs.edu.eg; Wagdy M. Eldehna  wagdy2000@gmail.com  Faculty of Pharmacy, Kafrelsheikh University, Kafrelsheikh, Egypt

 Supplemental data for this article can be accessed online at <https://doi.org/10.1080/14756366.2023.2234665>.

© 2023 The Author(s). Published by Informa UK Limited, trading as Taylor & Francis Group. This is an Open Access article distributed under the terms of the Creative Commons Attribution-NonCommercial License (<http://creativecommons.org/licenses/by-nc/4.0/>), which permits unrestricted non-commercial use, distribution, and reproduction in any medium, provided the original work is properly cited. The terms on which this article has been published allow the posting of the Accepted Manuscript in a repository by the author(s) or with their consent.

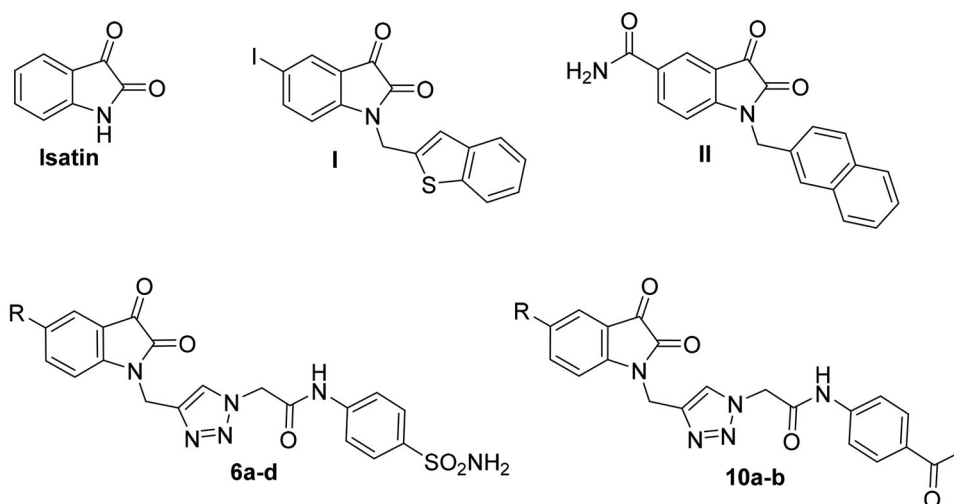


Figure 1. Structures of isatin and some reported main SARS-CoV protease inhibitors (I and II), as well as the target triazolo isatins (**6a-d** and **10a-b**).

Presently, the isatin motif (Figure 1) is highly valuable in the area of pharmaceutical chemistry and drug design¹⁵. Since it can be found and isolated from several natural resources and its synthetic accessibility, the isatin scaffold has been used to prepare novel derivatives with plethora of pharmacological properties such as anticancer^{16–19}, antibacterial^{20–21}, anti-tubercular^{22–24}, anti-malarial^{25–26}, antileishmanial^{27–28}, and antiviral activities²⁹. In particular, there has been a surge of interest in the recent decades to explore the biological effect of diverse isatin-based small molecules towards a wide range of pathogenic viruses. For example, the antiviral activities for diverse isatin derivatives were reported against HIV^{30–32}, arbovirus³³, chikungunya virus³⁴, herpes simplex virus (HSV)³⁵, coxsackievirus³⁶, poxvirus³⁷, and influenza virus³⁸.

Furthermore, many investigations have been conducted in order to afford isatin analogues as effective inhibitors of SARS-CoV main protease^{39–43}. Chen et al., in 2005, described the synthesis of *N*-substituted isatin derivatives endowed with a good inhibitory impact towards SARS-COV main protease in the low micromolar range (IC_{50} : 0.95–17.50 μ M). Among this series, compound **I** (Figure 1) emerged as the most promising inhibitor with IC_{50} equals 0.95 μ M⁴¹. Recently, Liu *et al* assessed the antiviral activity of other new *N*-substituted isatin-based molecules, by targeting SARS-CoV-2 main protease⁴³. The reported isatins demonstrated effective inhibitory activity against the tested protease, with compound **II** (Figure 1) standing out as the most promising candidate in that study (IC_{50} = 0.045 μ M).

Since previous studies spot the light on the potential activity of *N*-substituted isatins, we were inspired to design a novel set of derivatives (**6a-d** and **10a-b**) as potential inhibitors for SARS-CoV-2 main protease (Figure 1). The proposed derivatives were synthesised, characterised and evaluated using Fluorescence resonance energy transfer-based analysis to evaluate their inhibitory activity against SARS-CoV-2 main protease.

Results and discussion

Chemistry

The synthetic strategy was designed in order to retain the dione system which is characteristic to the isatin motif so that it could form an essential hydrogen bonding with important residues such as Cys145. Also, the *N*-substitution was decorated with the privileged triazole nucleus, which could enhance pharmacokinetic and pharmacodynamic profile, as well as incorporated an amide linker

that could achieve some important interactions. Lastly, the appended phenyl ring was grafted with a sulfamoyl functionality to afford the first series (**6a-d**), whereas in the second series the ketone group was exploited (**10a-b**), Figure 1.

The preparation of triazolo-isatins (**6a-d** and **10a-b**), utilised in this work, is demonstrated in Schemes 1 and 2. Acylation of the basic amino functionality in sulphanilamide **1** to afford 2-bromo-*N*-phenylacetamide **2**, was achieved through stirring in dry dioxane at room temperature and in the presence of K_2CO_3 , then, intermediate **2** was dissolved in dry dimethyl formamide and stirred with sodium azide at room temperature to furnish 2-azido-*N*-(4-sulfamoylphenyl)acetamide **3**. On the other hand, isatins **4a-d** were alkylated with propargyl bromide in dry acetonitrile and in presence of K_2CO_3 to produce the corresponding *N*-propargyl isatins **5a-d**, which further reacted with 2-azido-*N*-(4-sulfamoylphenyl)acetamide **3** through Azide-alkyne Huisgen cycloaddition in order to produce the target sulphonamide-tethered triazolo isatins **6a-d** (Scheme 1).

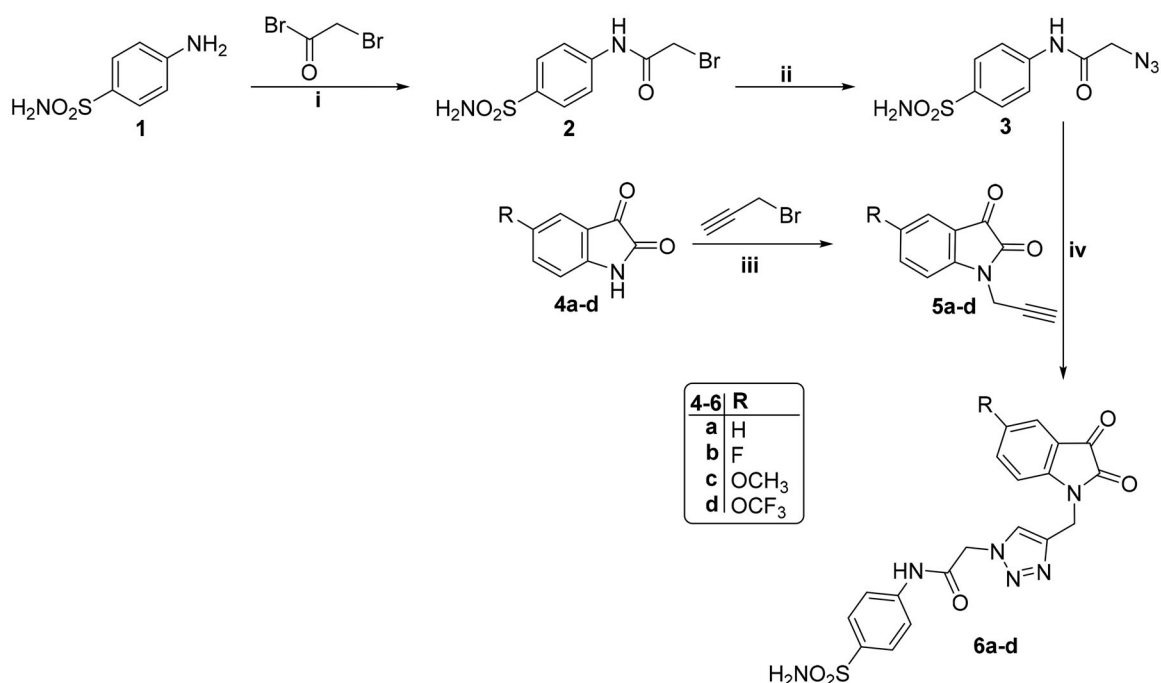
In Scheme 2, we aimed at replacing the sulphonamide functionality in the first series with a ketone group. *N*-(4-acetylphenyl)-2-azidoacetamide **9** was synthesised in the same way that 2-azido-*N*-(4-sulfamoylphenyl)acetamide **3** was. Thereafter, azide **9** was reacted with *N*-propargyl isatins **5a** and **5c** via the azide-alkyne cycloaddition click reaction to furnish the target triazolo isatins **10a-b** (Scheme 2). The structure of the prepared derivatives of triazolo isatin was well characterised and confirmed through interpretation of the spectral and the elemental analyses data.

Biological evaluation

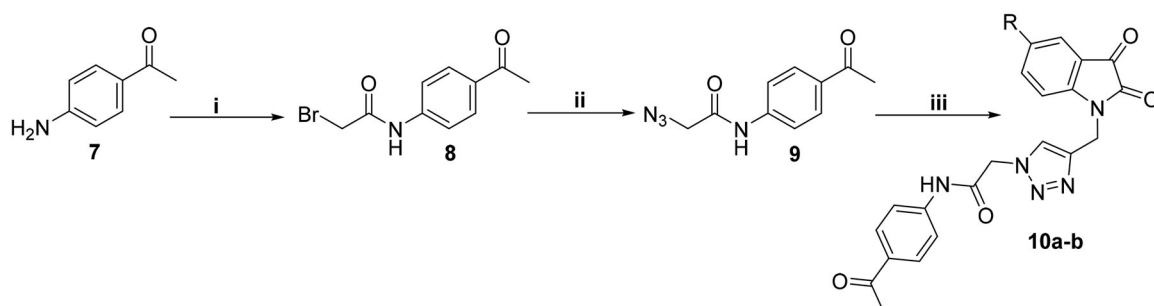
SARS-CoV-2 Mpro inhibitory assay

The newly synthesised triazolo isatins (**6a-d** and **10a-b**) were assessed for their inhibitory impact on the main protease of SARS-CoV-2, using **GC376** as a standard inhibitor. The inhibition data for the examined molecules were reported as median inhibition concentrations (IC_{50}) and displayed in Table 1, Figure S1.

The data listed in Table 1 disclosed that the examined 3CL-Pro was inhibited by the herein described triazolo isatins in a variable degree. The target sulphonamide-tethered triazolo isatins **6a-d** effectively inhibited 3CL-Pro with IC_{50} values spanning from 0.249 to 1.054 μ M. Compounds **6a-c** showed the ability to exert sub-micromolar inhibition; IC_{50} equal 0.562 \pm 0.005, 0.249 \pm 0.006 and 0.939 \pm 0.007 μ M, respectively, whereas compound **6d** displayed



Scheme 1. Reagent and conditions: (i) Dry dioxane, K_2CO_3 , stirring r.t., 12 h; (ii) NaN_3 , DMF, stirring r.t., 8 h; (iii) Dry acetonitrile, K_2CO_3 , stirring r.t., 10 h; (iv) DMF/ H_2O , $CuSO_4 \cdot 5H_2O$, sodium ascorbate, heating at $60^\circ C$, 7 h.



Scheme 2. Reagent and conditions: (i) Dry dioxane, K_2CO_3 , stirring r.t., 12 h; (ii) NaN_3 , DMF, stirring r.t., 8 h; (iii) 5a or 5c, DMF/ H_2O , $CuSO_4 \cdot 5H_2O$, sodium ascorbate, heating at $60^\circ C$, 7 h.

low-micromolar inhibitory activity ($IC_{50} = 1.054 \pm 0.053 \mu M$). Incorporation of unsubstituted isatin motif resulted in compound **6a** with good inhibitory activity ($IC_{50} = 0.562 \mu M$). Fluorine is exploited as an isostere for the hydrogen atom since its similar to hydrogen in terms of size and electronic characteristics. Triazole derivative **6b** bearing fluorine substituent at the isatin C-5 showed an increase in the 3CL-Pro inhibitory activity suggesting that the C-5 substitution is tolerated and also highlighting that the halogens incorporation may be advantageous. Moreover, grafting methoxy or trifluoromethoxy group led to compounds **6c** and **6d** with about 2-fold decreased activity ($IC_{50} = 0.939$, and $1.054 \mu M$, respectively) than their unsubstituted counterpart **6a**.

On the other hand, the introduction of acetyl instead of the sulphonamide functionality (compounds **10a** and **10b**) resulted in a dramatic decrease in the 3CL-Pro inhibitory action ($IC_{50} = 12.28$, and $17.075 \mu M$, respectively) hinting out that incorporation of the sulphonamide group is a crucial element for the activity.

The SARS-CoV-2 inhibitory assay (Cell-Based)

Since compound **6b** showed the best inhibitory effect against 3CL-Pro of SARS-CoV-2 established, its cellular antiviral activity was further assessed. Firstly, MTT assay was exploited to

determine the cytotoxicity of **6b** against VERO-E6 cell line. According to the data, **6b** has a favourable safety profile with a cytotoxicity concentration 50 (CC_{50}) value of $564.74 \mu g/ml$, which indicates that it has no significant impact on the survival of healthy, uninfected cells (Figure 2). Thereafter, the ability of **6b** to reduce the viability of SARS-CoV-2 cells was further investigated.

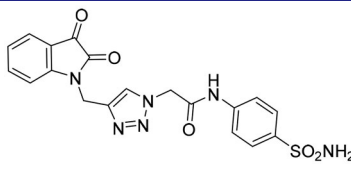
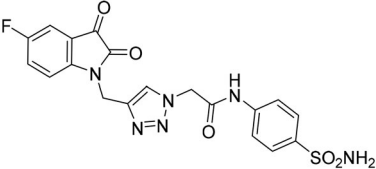
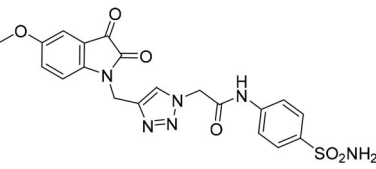
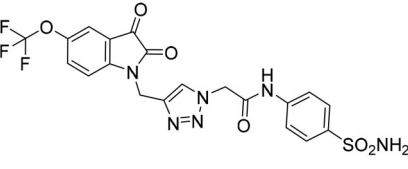
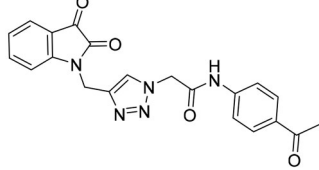
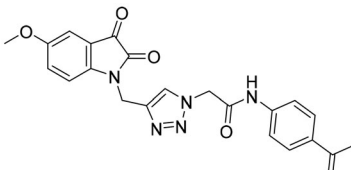
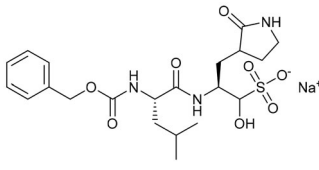
Remarkably, compound **6b** exerted promising cell growth inhibitory activity with $IC_{50} = 4.33 \mu g/ml$ that results in a safety index equals 130.4, suggesting that **6b** has good activity against SARS-CoV-2 *in-vitro* without causing toxicity to the host cells (Figure 2). This outcome is most likely associated with **6b**'s capacity to efficiently inhibit the 3CL-Pro enzyme, as previously described.

Molecular modeling studies

Docking studies

Molecular docking was proved to be a valuable tool to recognise the interactions of enzyme inhibitors⁴⁴⁻⁴⁸. Hence, we utilised molecular docking to gain an insight on the binding profile of isatin derivative **6b** with SARS-CoV-2 Mpro enzyme active site. As a start, redocking the co-crystallised ligand **GC-14** into its binding site was preformed to ensure the capability of the software to

Table 1. In vitro inhibitory effect of target triazolo isatins (**6a-d** and **10a-b**) against 3CL-Pro, using (**GC376**) as a standard drug.

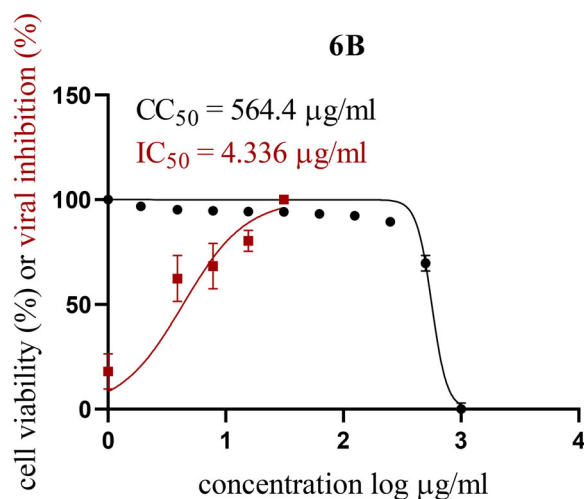
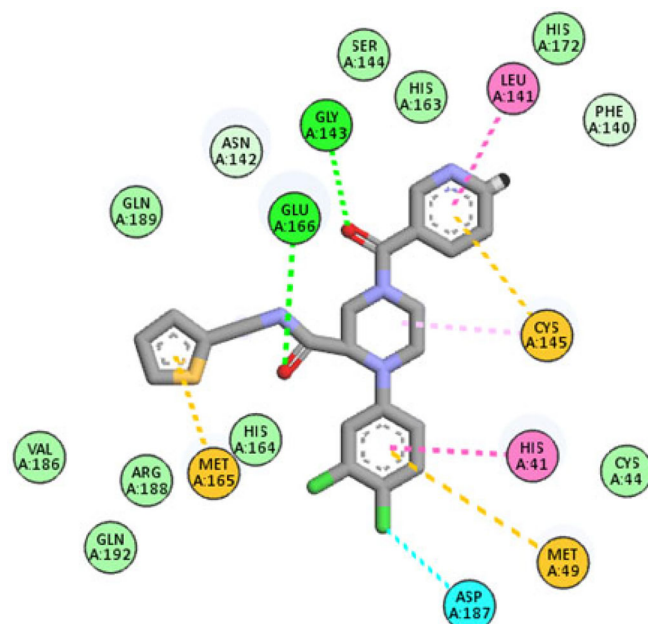
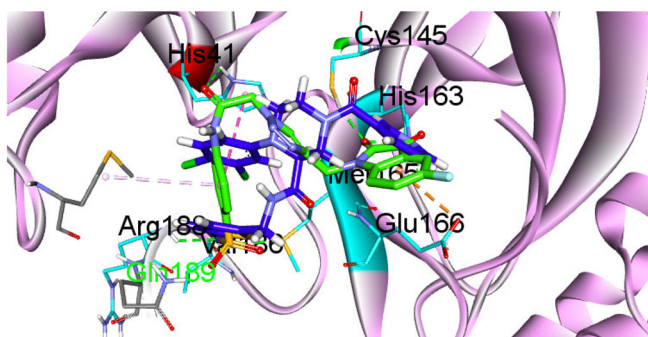
Comp.	R	^a IC ₅₀ (μM)
6a		0.562 ± 0.005
6b		0.249 ± 0.006
6c		0.939 ± 0.007
6d		1.054 ± 0.053
10a		12.28 ± 0.73
10b		17.075 ± 0.815
GC376		0.063 ± 0.001

^aMean from two different assays.

reproduce experimental pose in RMSD less than 1.5 Å. Since the calculated RMSD of the redocked pose was found to be 0.83, the docking protocol was considered valid. As depicted in **Figure 3**, the interaction of the co-crystallised ligand with the binding site could be summarised in its ability to form several interactions with the critical amino acids such as His 41, Met 49, Leu 141, Gly 143, Cys 145, Met 165 and Glu 166.

It's interesting to note that compound **6b** shared a similar binding mechanism with the co-crystallized ligand, as presented in **Figure 4**.

The isatin ring of **6b** interacted with Ser 144, Cys 145 through hydrogen bonding and one hydrophobic interaction with Glu166.

**Figure 2.** CC₅₀ and IC₅₀ values for isatin derivative **6b**.**Figure 3.** Redocking of the co-crystallised ligand GC-14 into SARS-CoV-2 Mpro binding site.**Figure 4.** Compound **6b** (in green) in 3D style overlaid with GC-14 (in blue).

Moreover, one hydrogen bond with His41 was formed through carbonyl of the amide linker formed. Furthermore, three hydrogen bonds with Met 165, Val 186 and Arg 188, were established through sulphonamide group in addition, the phenyl ring appended to the sulphonamide functionality formed two

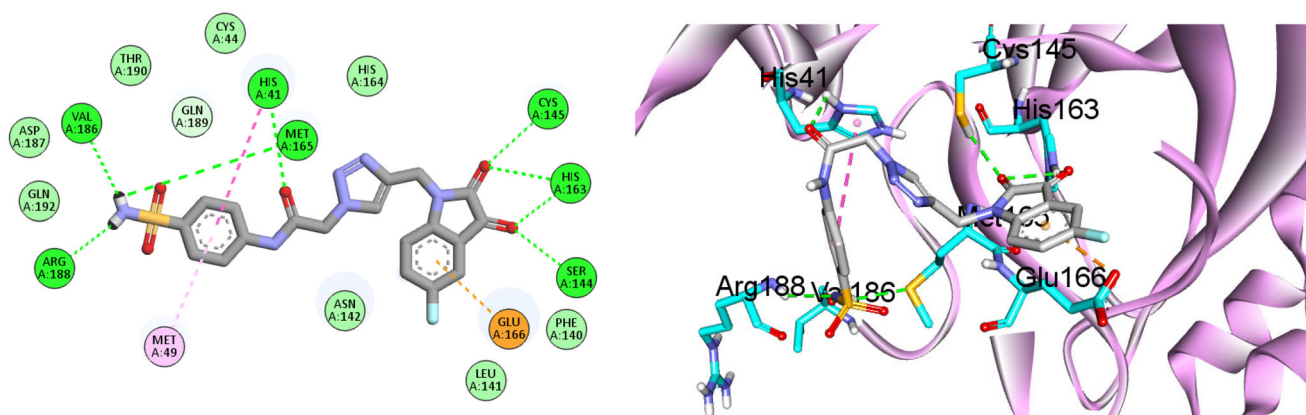


Figure 5. 2D and 3D interaction diagram of compound **6b** with SARS CoV-2 Mpro binding site.

hydrophobic interactions with His 41 and Met 49 (Figure 5). Finally, compound **6b** achieved binding energy of -10.7 Kcal/mol better than that for the co-crystallised (-9.8 Kcal/mol). To this end, the good binding mode and excellent docking score of compound **6b** highlights its ability to inhibit SARS CoV-2 Mpro through several types of interactions.

Molecular Dynamics

Further virtual investigations were achieved by molecular dynamic (MD) simulations studies. MD simulation provides various useful parameters for studying the dynamics of biological systems. Moreover, MD investigations might provide information about the binding affinity and intensity of docked complexes of a ligand and target proteins. To this end, the binding coordinate revealed by Mpro docking with isatin derivative **6b** was advanced to MD simulations. To provide a comparative mean for the effect of the newly synthesised triazolo isatin **6b** on the Mpro enzyme, the latter was subjected to MD using its apo form. Therefore, two MD simulations were conducted for 100 ns using GROMACS 5.1.1 software. As shown in Figure 6, triazolo isatin **6b** had the privilege of forming a stable complex with the Mpro enzyme, as indicated by its low RMSD values that averagely reached 1.5 Å. On the other hand, the RMSD of the apo Mpro enzyme reached an average value of 4.8 Å, indicating a high degree of flexibility suiting the Mpro intended function to process the viral polypeptide Figure 6. To this extent, the value decrease in the RMSD between the Mpro-**6b** complex and the apo Mpro highlights the great ability of triazolo isatin **6b** to strongly bind and inhibit the SARS CoV-2 Mpro enzyme.

Similar results were obtained from the RMSF analysis in which the residues of the apo protein demonstrated high fluctuations that reached an average of 4.3 Å. In comparison, the binding of compound **6b** to the Mpro residues, their stability increased significantly as indicated by average RMSF less than 1.6 Å, Figure 7. To summarise, the MDs results highlight the ability of triazolo isatin **6b** to inhibit the SARS CoV-2 Mpro enzyme through forming a stable complex within the Mpro active site, as consistent with the enzyme assay.

Conclusion

The preparation of isatin-triazole hybrids was successfully facile through click chemistry allowing the development of novel compounds as Main protease (Mpro) inhibitors. Sulphonamide tethered derivatives showed better activity than the acetophenone derivatives, especially compound **6b** which exhibited sub-

micromolar enzyme inhibitory activity in FRET assay. Thereafter, triazolo isatin **6b**'s antiviral activity was demonstrated by its capacity to inhibit the proliferation of viral cells with an IC_{50} value of 4.33 µg/ml. Notably, **6b** exerted non-significant toxicity towards VERO-E6 cells ($CC_{50} = 564.74$ µg/ml) revealing a favourable safety profile with selectivity index equals 130.4. This remarkable observation was supported by molecular docking and molecular dynamic simulation which showed the interaction of **6b** with several important amino acid residues in the binding site of Mpro and the stability of the formed interactions between the compound and the active site. In particular, the formation of several hydrogen bonds with amino acids involved in the catalytic activity of the enzyme through the alpha-ketoamide moiety and sulphonyl amide function group explains the superior activity of benzenesulfonylamide tethered derivatives **6** over acetophenone derivatives **10**. Hence, **6b** could be further developed as anti-SARS-CoV-2 agent after performing more extensive studies.

Experimental

Chemistry

General

The solvents and reagents used in the reactions were commercially sourced and not purified further. A Stuart melting point device was used to measure melting points that was uncorrected. NMR spectra were attained using a JEOL ECA 500 NMR Spectrometer (500 MHz 1H and 126 MHz ^{13}C NMR), while elemental analysis (% C, H, and N) was accomplished using a PerkinElmer 2400 CHNS analyser. Reaction progress and product mixtures were regularly monitored through thin layer chromatography (TLC) using Aluminium sheets pre-coated with silica gel 60 F254 purchased from Merk.

Synthesis of intermediates 2-bromo-*N*-phenylacetamides **2** and **8**

To a suspension of 4-aminobenzenesulfonamide **1** or 4'-aminoacetophenone **2** (20 mmol) in dry dioxane (15 ml) and K_2CO_3 (5.5 g, 40 mmol) at $0^\circ C$, bromoacetyl bromide (4.42 g, 22 mmol) was added dropwise and the mixture was incubated at r.t. with stirring for 12 h. Then, ice-water was added to the reaction mixture, and the precipitate that developed was filtered out, dried and recrystallized from ethanol to produce 2-bromo-*N*-phenylacetamides **2** and **8** with 75% and 80% yield, respectively.⁴⁹

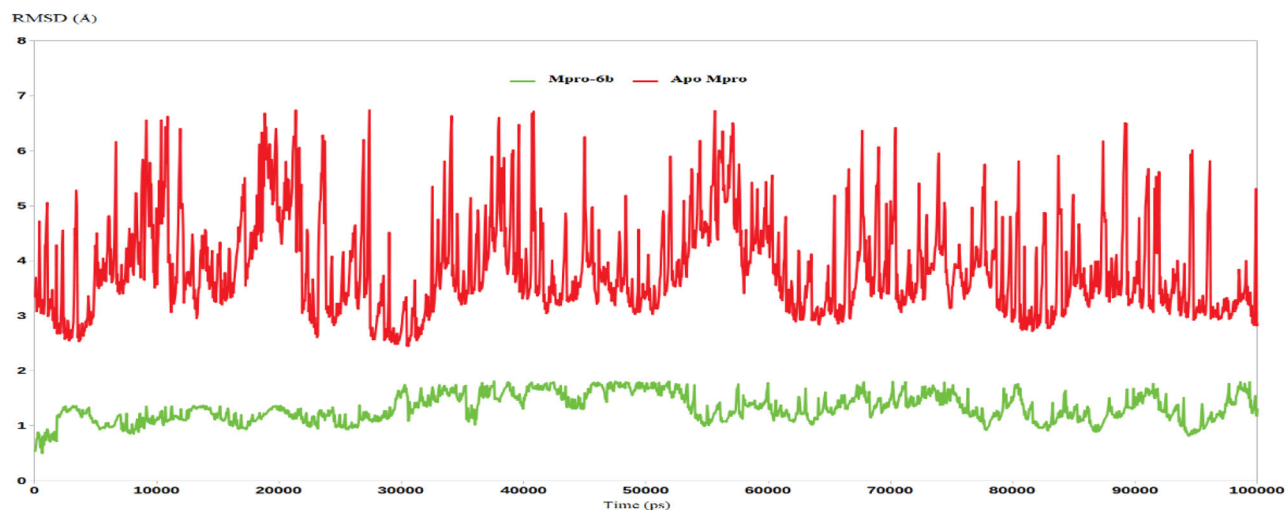


Figure 6. RMSD analysis for the MD simulations.

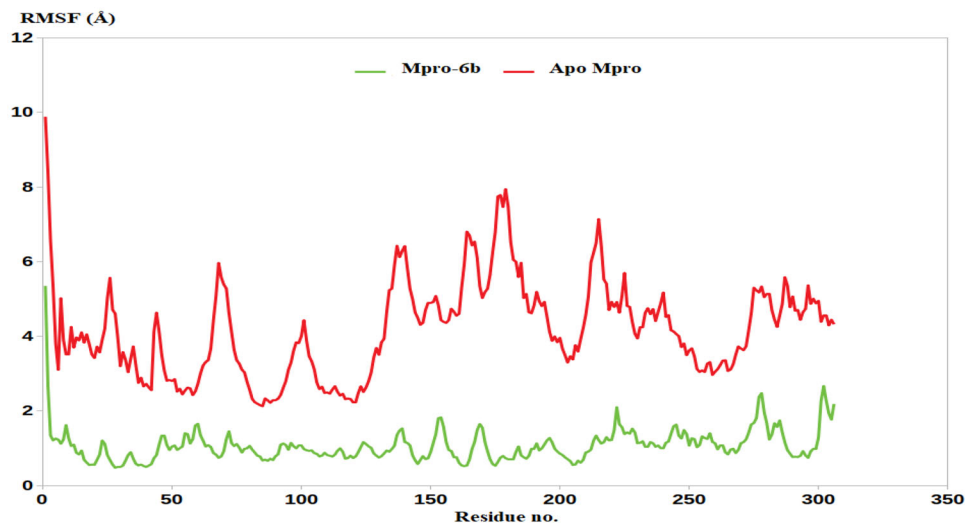


Figure 7. RMSF analysis for the MD simulations.

Synthesis of intermediates 2-azido-*N*-phenylacetamides **3** and **9**

To a solution of 2-bromo-*N*-phenylacetamides **2** and **8** (15 mmol) in dry DMF (15 ml), sodium azide (2.9 g, 45 mmol) was added. The reaction mixture was incubated at r.t. while stirring for 8 h, and then water (75 ml) was added, and the reaction mixture was extracted with CH₂Cl₂ (3 × 20 ml). The organic layer was washed with brine, and dried over anhydrous Na₂SO₄, then evaporated under reduced pressure to furnish intermediates 2-azido-*N*-phenylacetamides **3** and **9** which used in the next step forthwith without further purification^{50–51}. Yield: 73% (**3**); 70% (**9**).

Synthesis of *N*-propargyl isatins **5a-d**

A solution of isatin derivatives 4a-d (20 mmol), propargyl bromide (22 mmol), and K₂CO₃ (5.5 g, 40 mmol) in dry acetonitrile (15 ml) was incubated at r.t. while stirring for 10 h. Afterward, ethyl acetate (3 × 15 ml) was used to extract the reaction mixture after it had been poured into water. The organic layer was dried over anhydrous MgSO₄ and concentrated at reduced pressure after

being washed with brine to yield *N*-propargyl isatins **5a-d**. The yields were 72%, 78%, 70%, and 75% for **5a-d**, respectively.

1-(Prop-2-yn-1-yl)isatin (5a). Yield = 78%, Orange crystals, melting point = 160–162 °C (reported melting point = 158–160 °C)⁵².

5-Fluoro-1-(prop-2-yn-1-yl)isatin (5b). Yield = 72%, Red crystals, melting point = 128–130 °C (reported melting point = 124–125 °C)⁵³.

5-Methoxy-1-(prop-2-yn-1-yl)isatin (5c). Yield = 75%, Red crystals, melting point = 131–133 °C (reported melting point = 130–132 °C)⁵⁴.

1-(Prop-2-yn-1-yl)-5-(trifluoromethoxy)isatin (5d). Orange crystals, yield = 70%, melting point = 91–92 °C; ¹H NMR (500 MHz, DMSO-*d*₆) δ (ppm): 3.37 (s, 1H, -C≡CH), 4.59 (d, 2H, N-CH₂, *J* = 2.0 Hz), 7.34 (d, 1H, Aromatic-H, *J* = 8.8 Hz), 7.64 (s, 1H, Aromatic-H), 7.76

(d, 1H, Aromatic-H, $J=8.8$ Hz); Anal. Calcd. for $C_{12}H_6F_3NO_3$: C, 53.54; H, 2.25; N, 5.20; found C, 53.68; H, 2.24; N, 5.17.

General procedure for synthesis of target inhibitors 6a-d and 10a-b

A solution containing 2-azido-*N*-phenylacetamides **3** and **9** (2 mmol) in 5 ml of a mixture of DMF and H₂O (4:1) was prepared. To this solution, *N*-propargyl isatins 5a-d (2 mmol), CuSO₄·5H₂O (1 mmol), and sodium ascorbate (2 mmol) were added. The resulting reaction mixture was stirred at 60 °C for 7 h. After the reaction was complete, the mixture was poured onto crushed ice, filtered, and dried under reduced pressure. The resulting product was crystallised from ethanol to yield the target compounds **6a-d** and **10a-b**.

2-(4-((2,3-Dioxindolin-1-yl)methyl)-1H-1,2,3-triazol-1-yl)-N-(4-sulfamoylphenyl)acetamide (6a). Yield (75%); Orange crystals; melting point = 280–282 °C; ¹H NMR (DMSO-*d*₆, 500 MHz) δ (ppm): 4.99 (s, 2H, -CH₂), 5.33 (s, 2H, -CH₂), 7.11 (t, 1H, Aromatic-H, $J=8.0$ Hz), 7.18 (d, 1H, Aromatic-H, $J=8.0$ Hz), 7.27 (s, 2H, SO₂NH₂), 7.52 (d, 1H, Aromatic-H, $J=7.0$ Hz), 7.62 (t, 1H, Aromatic-H, $J=7.0$ Hz), 7.69 (d, 2H, Aromatic-H, $J=8.5$ Hz), 7.75 (d, 2H, Aromatic-H, $J=8.5$ Hz), 8.19 (s, 1H, Aromatic-H), 10.79 (s, 1H, NH); ¹³C NMR (DMSO-*d*₆, 126 MHz) δ ppm: 35.04, 52.29, 111.25, 117.62, 118.90, 123.45, 124.54, 125.36, 126.90, 138.17, 138.91, 141.26, 141.36, 150.22, 157.88, 164.80, 183.11; Anal. Calcd. for C₁₉H₁₆N₆O₅S: C, 51.81; H, 3.66; N, 19.08; found C, 52.01; H, 3.64; N, 19.02.

2-(4-((5-Fluoro-2,3-dioxindolin-1-yl)methyl)-1H-1,2,3-triazol-1-yl)-N-(4-sulfamoylphenyl) acetamide (6b). Yield (75%); Red crystals; melting point = 271–273 °C; ¹H NMR (DMSO-*d*₆, 500 MHz) δ (ppm): 4.99 (s, 2H, -CH₂), 5.33 (s, 2H, -CH₂), 7.20 (dd, 1H, Aromatic-H, $J=8.0, 4.0$ Hz), 7.26 (s, 2H, SO₂NH₂), 7.47–7.53 (m, 2H, Aromatic-H), 7.68 (d, 2H, Aromatic-H, $J=9.0$ Hz), 7.75 (d, 2H, Aromatic-H, $J=9.0$ Hz), 8.18 (s, 1H, Aromatic-H), 10.78 (s, 1H, NH); ¹³C NMR (DMSO-*d*₆, 126 MHz) δ ppm: 35.11, 52.29, 111.43, 111.62, 112.63, 112.68, 118.54, 118.60, 118.89, 123.92, 124.14, 125.38, 126.89, 138.92, 141.26, 146.43, 157.64, 157.92, 159.55, 164.78, 182.49; Anal. Calcd. for C₁₉H₁₅FN₆O₅S: C, 49.78; H, 3.30; N, 18.33; found C, 49.93; H, 3.29; N, 18.26.

2-(4-((5-Methoxy-2,3-dioxindolin-1-yl)methyl)-1H-1,2,3-triazol-1-yl)-N-(4-sulfamoylphenyl) acetamide (6c). Yield (75%); Reddish brown crystals; melting point = 295–297 °C; ¹H NMR (DMSO-*d*₆, 500 MHz) δ (ppm): 3.74 (s, 3H, OCH₃), 4.96 (s, 2H, -CH₂), 5.33 (s, 2H, -CH₂), 7.11–7.24 (m, 2H, Aromatic-H), 7.26 (s, 2H, SO₂NH₂), 7.69 (d, 2H, Aromatic-H, $J=9.0$ Hz), 7.75–7.77 (m, 3H, Aromatic-H), 8.17 (s, 1H, Aromatic-H), 10.79 (s, 1H, NH); Anal. Calcd. for C₂₀H₁₈N₆O₆S: C, 51.06; H, 3.86; N, 17.86; found C, 50.86; H, 3.88; N, 17.95.

2-(4-((2,3-Dioxo-5-(trifluoromethoxy)indolin-1-yl)methyl)-1H-1,2,3-triazol-1-yl)-N-(4-sulfamoylphenyl)acetamide (6d). Yield (75%); Light brown crystals; melting point = 283–285 °C; ¹H NMR (DMSO-*d*₆, 500 MHz) δ (ppm): 5.01 (s, 2H, -CH₂), 5.34 (s, 2H, -CH₂), 7.26 (s, 2H, SO₂NH₂), 7.29 (d, 1H, Aromatic-H, $J=8.0$ Hz), 7.61 (s, 1H, Aromatic-H), 7.69–7.71 (m, 3H, Aromatic-H), 7.75 (d, 2H, Aromatic-H, $J=9.0$ Hz), 8.19 (s, 1H, Aromatic-H), 10.79 (s, 1H, NH); Anal. Calcd. for C₂₀H₁₅F₃N₆O₆S: C, 45.81; H, 2.88; N, 16.03; found C, 45.93; H, 2.87; N, 15.96.

N-(4-Acetylphenyl)-2-(4-((2,3-dioxindolin-1-yl)methyl)-1H-1,2,3-triazol-1-yl)acetamide (10a). Yield (71%); Yellow crystals; melting point = 231–233 °C; ¹H NMR (DMSO-*d*₆, 500 MHz) δ (ppm): 2.51 (s, 3H, COCH₃), 4.99 (s, 2H, -CH₂), 5.34 (s, 2H, -CH₂), 7.11 (t, 1H, Aromatic-H, $J=7.5$ Hz), 7.18 (d, 1H, Aromatic-H, $J=8.0$ Hz), 7.55 (d, 1H, Aromatic-H, $J=7.5$ Hz), 7.62 (t, 1H, Aromatic-H, $J=8.0$ Hz), 7.67 (d, 2H, Aromatic-H, $J=9.0$ Hz), 7.92 (d, 2H, Aromatic-H, $J=8.5$ Hz), 8.19 (s, 1H, Aromatic-H), 10.78 (s, 1H, NH); ¹³C NMR (DMSO-*d*₆, 126 MHz) δ ppm: 26.48, 35.02, 52.32, 111.23, 117.60, 118.54, 123.42, 124.51, 125.33, 129.62, 132.17, 138.13, 141.35, 142.64, 150.20, 157.86, 164.79, 183.09, 196.58; Anal. Calcd. for C₂₁H₁₇N₅O₄: C, 62.53; H, 4.25; N, 17.36; found C, 62.38; H, 4.28; N, 17.43.

N-(4-Acetylphenyl)-2-(4-((5-methoxy-2,3-dioxindolin-1-yl)methyl)-1H-1,2,3-triazol-1-yl)acetamide (10b). Yield (75%); Yellow crystals; melting point = 245–247 °C; ¹H NMR (DMSO-*d*₆, 500 MHz) δ (ppm): 2.51 (s, 3H, COCH₃), 3.74 (s, 3H, OCH₃), 4.96 (s, 2H, -CH₂), 5.33 (s, 2H, -CH₂), 7.11–7.14 (m, 2H, Aromatic-H), 7.22 (d, 1H, Aromatic-H, $J=9.0$ Hz), 7.67 (d, 2H, Aromatic-H, $J=9.0$ Hz), 7.92 (d, 2H, Aromatic-H, $J=9.0$ Hz), 8.18 (s, 1H, Aromatic-H), 10.79 (s, 1H, NH); ¹³C NMR (DMSO-*d*₆, 126 MHz) δ ppm: 26.49, 35.01, 52.32, 55.93, 109.23, 112.34, 118.06, 118.55, 119.04, 123.93, 125.31, 129.63, 132.18, 142.65, 144.02, 155.87, 157.90, 162.37, 164.81, 183.37, 196.60; Anal. Calcd. for C₂₂H₁₉N₅O₅: C, 60.97; H, 4.42; N, 16.16; found C, 61.14; H, 4.42; N, 16.16.

Biological evaluations

Protein expression and purification for SARS-CoV-2 Mpro

The DNA sequence of the SARS-CoV-2 Main protease (Mpro) was acquired from the complete genome of SARS-CoV-2 (GenBank MN908947.3). The gene that encodes the protein was optimised for expression in *Escherichia coli* (*E. coli*) and synthesised by Bio Basic Inc (Konrad Crescent, Canada). The synthesised gene was inserted into a pET-28a(+) plasmid with a C-terminal His tag. Competent *E. coli* BL21 (DE3) cells were transformed using this plasmid (New England Biolabs). The transformed cells were grown at a temperature of 37 °C in a medium made of terrific broth (TB) with the addition of 50 µg/mL of the antibiotic Kanamycin and 1% glucose. Protein production was induced after reaching OD₆₀₀ of 0.6 by the addition of 0.5 mM isopropyl β -D-1-thiogalactopyranoside (IPTG), then the cells were incubated at 16 °C and 180 rpm overnight. The cells were then collected by centrifuging them at 7000 rpm for 30 min at 4 °C, resuspended in a lysis buffer, and then sonicated to lyse them. Finally, they were centrifuged at 12000 rpm for 40 min at 4 °C to remove the remaining cell debris. The His-tagged protein was purified from the supernatant using affinity TALON Superflow resin (Cytiva, Marlborough, USA) and eluted with an elution buffer containing 50 mM TRIS, 300 mM imidazole, and 150 mM NaCl. SDS-PAGE was used to determine the protein's degree of purity (see Figure S1), and the pure protein was dialysed and concentrated using a 10K Pierce™ Protein Concentrator (Thermo Scientific).

Enzyme inhibition assay

The enzyme inhibition experiment was conducted in 96-well, black microtiter plates with a total volume of 200 µl. A final concentration of 20 nM of the SARS-CoV-2 Mpro enzyme was used. The compounds being assessed, along with GC376 as a standard inhibitor, were pre-incubated with the enzyme at different concentrations in an assay buffer consisting of 20 mM TRIS, 1 mM EDTA, 150 mM NaCl, 1 mM DTT and the pH was adjusted to 7.3. A

FRET substrate, Dabcyl-KTSAVLQSGFRKME-EDANS, was added to the mixture at final concentration of 10 μ M and incubated in the dark for 3 h at room temperature. Fluorescence signals of released EDANS were estimated using a Spectrofluorometer with microplate reader accessory (Cary Eclipse, Agilent Technologies) at (excitation/emission, 355 nm/460 nm), and the blank was determined by measuring the entire reaction mixture without the enzyme. The obtained data was plotted and analysed to determine the IC₅₀ values of the tested compounds using nonlinear regression with a variable slope.

MTT cytotoxicity assay towards VERO-E6 cells

The cytotoxic impact of triazolo isatin derivative **6b** was tested in VERO-E6 cells by using the 3-(4,5-dimethylthiazol-2-yl)-2,5-diphenyltetrazolium bromide (MTT) method with minor modifications^{55,56}. The procedures were provided in the [Supplementary Materials](#).

Cell-Based SARS-CoV-2 inhibitory assay

The cellular antiviral activity of compound **6b** against SARS-CoV-2 was assessed and the IC₅₀ value was determined as described previously^{57–59}. The procedures were provided in the [Supplementary Materials](#).

Molecular modelling studies

Molecular docking

Vina Autodock software was used to perform docking studies on compound **6b**⁶⁰. The protein data bank (PDB) was utilised to download the 3D co-ordinates of SARS CoV-2 Mpro bound to an experimental inhibitor (PDB ID: 8ACL)⁶¹. The 3D structure of our proposed molecule was created by the Biovia discovery visualiser after it was sketched by ChemDraw. M.G.L 1.5.7 tools were used in the generation of the needed pdbqt format files, since it is mandatory for both receptor and ligands to be in pdbqt format as essential required by Vina Autodock. Moreover, the binding pocket was built using a grid box encompassing the binding of the co-crystallised ligand with dimensions of 22, 22, and 22, respectively, in the three axes. To ensure a valid docking approach, initial docking of the co-crystallised coordinates to the pre-determined binding domain was conducted. Finally, compound **6b** was docked into the validated binding domain of SARS CoV-2 Mpro enzyme. The Biovia discovery studio 2021 free visualiser was used to create 2D and 3D interactions for the docked pose to visualise the interaction of **6b** with the active site of Mpro.

Molecular Dynamics

Two molecular dynamic simulations (MDS) were conducted for 100 ns exploiting software of GROMACS 5.1.1⁶². The retrieved docking coordinates of the Mpro enzyme in-complex with triazolo isatin **6b** and the apo mpro enzyme. The receptor and ligand topologies were generated by PDB2gmx (embedded in GROMACS) and GlycoBioChem PRODRG2 Server respectively, both under GROMOS96 force field⁶³. After rejoining ligands and receptor topologies to generate two systems, the typical molecular dynamics scheme of GROMACS was applied for all the systems. This includes, solvation, neutralisation, energy minimisation under GROMOS96 43a1 force field and two stages of equilibration (NVT and NPT)^{64–67}. Finally, unrestricted production stage of 100 ns was

applied for the two systems with the Particle Mesh Ewald (PME) method implemented to compute the long-range electrostatic values using 12 Å cut-off and 12 Å Fourier spacing. The stability of the complexes was judged using RMSD and RMSF values calculated from the MDS trajectories from the production step.

Disclosure statement

CT Supuran is Editor-in-Chief of the Journal of Enzyme Inhibition and Medicinal Chemistry. He was not involved in the assessment, peer review, or decision-making process of this paper. The authors have no relevant affiliations of financial involvement with any organisation or entity with a financial interest in or financial conflict with the subject matter or materials discussed in the manuscript. This includes employment, consultancies, honoraria, stock ownership or options, expert testimony, grants or patents received or pending, or royalties.

Funding

This paper is based upon work supported by Science, Technology & Innovation Funding Authority (STDF) under grant number [44025].

ORCID

Mai H. ElNaggar  <http://orcid.org/0000-0001-5481-2053>
 Abdullah A. Elgazar  <http://orcid.org/0000-0002-5851-3306>
 Claudiu T. Supuran  <http://orcid.org/0000-0003-4262-0323>
 Wagdy M. Eldehna  <http://orcid.org/0000-0001-6996-4017>

References

- Cucinotta D, Vanelli M. WHO declares COVID-19 a pandemic. *Acta Biomed.* 2020;91:157–160.
- Mori M, Capasso C, Carta F, Donald WA, Supuran CT. A deadly spillover: SARS-CoV-2 outbreak. *Expert Opin Ther Pat.* 2020;30(7):481–485.
- CDC. COVID-19 Treatments and Medications. 2023. <https://www.cdc.gov/coronavirus/2019-ncov/your-health/treatments-for-severe-illness.html>
- CDC. Interim Clinical Considerations for COVID-19 Treatment in Outpatients. 2023. <https://www.cdc.gov/coronavirus/2019-ncov/hcp/clinical-care/outpatient-treatment-overview.html>
- Supuran CT. Coronaviruses. *Expert Opin Ther Pat.* 2021;31(4):291–294.
- Deniz S, Uysal TK, Capasso C, Supuran CT, Ozensoy Guler O. Is carbonic anhydrase inhibition useful as a complementary therapy of Covid-19 infection? *J Enzyme Inhib Med Chem.* 2021;36(1):1230–1235.
- Macip G, Garcia-Segura P, Mestres-Truyol J, Saldivar-Espinoza B, Pujadas G, Garcia-Vallvé S. A review of the current landscape of SARS-CoV-2 main protease inhibitors: have we hit the bullseye yet? *IJMS.* 2021;23(1):259.
- Yan S, Wu G. Spatial and temporal roles of SARS-CoV PLpro—A snapshot. *Faseb J.* 2021;35(1):e21197.
- Jin Z, Du X, Xu Y, Deng Y, Liu M, Zhao Y, Zhang B, Li X, Zhang L, Peng C, et al. Structure of M(pro) from SARS-CoV-2 and discovery of its inhibitors. *Nature.* 2020;582(7811):289–293.
- Zhong N, Zhang S, Zou P, Chen J, Kang X, Li Z, Liang C, Jin C, Xia B. Without its N-finger, the main protease of severe

- acute respiratory syndrome coronavirus can form a novel dimer through its C-terminal domain. *J Virol.* 2008;82(9):4227–4234.
11. a) Capasso C, Nocentini A, Supuran CT. Protease inhibitors targeting the main protease and papain-like protease of coronaviruses. *Expert Opin Drug Discov.* 2022;17(6):547–557. b) Nocentini A, Capasso C, Supuran CT. Perspectives on the design and discovery of α -ketoamide inhibitors for the treatment of novel coronavirus: where do we stand and where do we go? *Expert Opin Drug Discov.* 2022;17(6):547–557.
 12. a) Ma C, Sacco MD, Hurst B, Townsend JA, Hu Y, Szeto T, Zhang X, et al. Boceprevir, GC-376, and calpain inhibitors II, XII inhibit SARS-CoV-2 viral replication by targeting the viral main protease. *Cell Res.* 2020;30(8):678–692. b) Vuong W, Khan MB, Fischer C, Arutyunova E, Lamer T, Shields J, Saffran HA, et al. Feline coronavirus drug inhibits the main protease of SARS-CoV-2 and blocks virus replication. *Nat Commun.* 11(1)2020;4282.
 13. a) Joyce RP, Hu VW and Wang J. The history, mechanism, and perspectives of nirmatrelvir (PF-07321332): an orally bioavailable main protease inhibitor used in combination with ritonavir to reduce COVID-19-related hospitalizations. *Med Chem Res.* 2022;31(10):1637–1646. b) Singh J, Petter RC, Baillie TA, Whitty A. The resurgence of covalent drugs. *Nat Rev Drug Discovery.* 2011;10:307–317.
 14. Bauer RA. Covalent inhibitors in drug discovery: from accidental discoveries to avoided liabilities and designed therapies. *Drug Discov Today.* 2015;20(9):1061–1073.
 15. Brandao P, Marques C, Burke AJ, Pineiro M. The application of isatin-based multicomponent-reactions in the quest for new bioactive and druglike molecules. *Eur J Med Chem.* 2021;211:113102.
 16. Eldehna WM, El Hassab MA, Abo-Ashour MF, Al-Warhi T, Elaasser MM, Safwat NA, Suliman H, Ahmed MF, Al-Rashood ST, Abdel-Aziz HA, et al. Development of isatin-thiazolo [3, 2-a] benzimidazole hybrids as novel CDK2 inhibitors with potent in vitro apoptotic anti-proliferative activity: synthesis, biological and molecular dynamics investigations. *Bioorg Chem.* 2021;110:104748.
 17. Eldehna WM, Al-Wabli RI, Almutairi MS, Keeton AB, Piazza GA, Abdel-Aziz HA, Attia MI. Synthesis and biological evaluation of certain hydrazonoindolin-2-one derivatives as new potent anti-proliferative agents. *J Enzyme Inhib Med Chem.* 2018;33(1):867–878.
 18. a) Taghour MS, Elkady H, Eldehna WM, El-Deeb NM, Kenawy AM, Elkaeed EB, Alsouk AA, Alesawy MS, Metwaly AM, and Eissa IH. Design and synthesis of thiazolidine-2, 4-diones hybrids with 1, 2-dihydroquinolones and 2-oxindoles as potential VEGFR-2 inhibitors: in-vitro anticancer evaluation and in-silico studies. *J Enzyme Inhib Med Chem.* 2022;37(1):1903–1917. b) Eldehna WM, Fares M, Ibrahim HS, Alsherbiny MA, Aly MH, Ghabbour HA, Abdel-Aziz HA. Synthesis and cytotoxic activity of biphenylurea derivatives containing indolin-2-one moieties. *Molecules.* 2016;21(6):762.
 19. Al-Warhi T, Abo-Ashour MF, Almahli H, Alotaibi OJ, Al-Sanea MM, Al-Ansary GH, Ahmed HY, Elaasser MM, Eldehna WM, Abdel-Aziz HA. Novel [(N-alkyl-3-indolylmethylene) hydrazono] oxindoles arrest cell cycle and induce cell apoptosis by inhibiting CDK2 and Bcl-2: synthesis, biological evaluation and in silico studies. *J Enzyme Inhib Med Chem.* 2020;35(1):1300–1309.
 20. Guo H. Isatin derivatives and their anti-bacterial activities. *Eur J Med Chem.* 2019;164:678–688.
 21. Al-Warhi T, Elimam DM, Elsayed ZM, Abdel-Aziz MM, Maklad RM, Al-Karmalawy AA, Afarinkia K, Abourehab MA, Abdel-Aziz HA, Eldehna WM. Development of novel isatin thiazolopyrazoline hybrids as promising antimicrobials in MDR pathogens. *RSC Adv.* 2022;12(48):31466–31477.
 22. a) Xu Z, Zhang S, Gao C, Fan J, Zhao F, Lv Z-S, Feng L-S. Isatin hybrids and their anti-tuberculosis activity. *Chin Chem Lett.* 2017;28(2):159–167. b) Abdel-Aziz HA, Ghabbour HA, Eldehna WM, Qabeel MM, Fun H-K. Synthesis, crystal structure, and biological activity of cis/trans amide rotomers of (Z)-N'-(2-Oxoindolin-3-ylidene) formohydrazide. *J Chem.* 2014;2014:760434.
 23. Abdelrahman MA, Almahli H, Al-Warhi T, Majrashi TA, Abdel-Aziz MM, Eldehna WM, Said MA. Development of novel isatin-tethered quinolines as anti-tubercular agents against multi and extensively drug-resistant mycobacterium tuberculosis. *Molecules.* 2022;27(24):8807.
 24. Elsayed ZM, Eldehna WM, Abdel-Aziz MM, El Hassab MA, Elkaeed EB, Al-Warhi T, Abdel-Aziz HA, Abou-Seri SM, Mohammed ER. Development of novel isatin–nicotinohydrazide hybrids with potent activity against susceptible/resistant Mycobacterium tuberculosis and bronchitis causing-bacteria. *J Enzyme Inhib Med Chem.* 2021;36(1):384–393.
 25. Chiyanzu I, Clarkson C, Smith PJ, Lehman J, Gut J, Rosenthal PJ, Chibale K. Design, synthesis and anti-plasmodial evaluation in vitro of new 4-aminoquinoline isatin derivatives. *Bioorg Med Chem.* 2005;13(9):3249–3261.
 26. Thakur RK, Joshi P, Baranwal P, Sharma G, Shukla SK, Tripathi R, Tripathi RP. Synthesis and antiplasmodial activity of glyco-conjugate hybrids of phenylhydrazono-indolinones and glycosylated 1, 2, 3-triazolyl-methyl-indoline-2, 3-diones. *Eur J Med Chem.* 2018;155:764–771.
 27. Khatoun S, Aroosh A, Islam A, Kalsoom S, Ahmad F, Hameed S, Abbasi SW, Yasinzi M, Naseer MM. Novel coumarin-isatin hybrids as potent antileishmanial agents: synthesis, in silico and in vitro evaluations. *Bioorg Chem.* 2021;110:104816.
 28. Sabt A, Eldehna WM, Ibrahim TM, Bekhit AA, Batran RZ. New antileishmanial quinoline linked isatin derivatives targeting DHFR-TS and PTR1: design, synthesis, and molecular modeling studies. *Eur J Med Chem.* 2023;246:114959.
 29. Elsaman T, Mohamed MS, Mohamed Eltayib E, Abdel-Aziz HA, Abdalla AE, Munir MU, Mohamed MA. Isatin derivatives as broad-spectrum antiviral agents: the current landscape. *Med Chem Res.* 2022;31(2):244–273.
 30. Pandeya SN, Yogeewari P, Sriram D, De Clercq E, Pannecouque C, Witvrouw M. Synthesis and screening for anti-HIV activity of some N-Mannich bases of isatin derivatives. *Chemotherapy.* 1999;45(3):192–196.
 31. Banerjee D, Yogeewari P, Bhat P, Thomas A, Srividya M, Sriram D. Novel isatinyl thiosemicarbazones derivatives as potential molecule to combat HIV-TB co-infection. *Eur J Med Chem.* 2011;46(1):106–121.
 32. Bal TR, Anand B, Yogeewari P, Sriram D. Synthesis and evaluation of anti-HIV activity of isatin β -thiosemicarbazone derivatives. *Bioorg Med Chem Lett.* 2005;15(20):4451–4455.
 33. De Moraes Gomes PAT, Pena LJ, Leite ACL. Isatin derivatives and their antiviral properties against arboviruses: a review. *Mini Rev Med Chem.* 2019;19(1):56–62.
 34. Mishra P, Kumar A, Mamidi P, Kumar S, Basantray I, Saswat T, Das I, Nayak TK, Chattopadhyay S, Subudhi BB, et al. Inhibition of Chikungunya virus replication by 1-[(2-Methylbenzimidazol-1-yl) Methyl]-2-Oxo-Indolin-3-ylidene] Amino] Thiourea(MBZM-N-IBT). *Sci Rep.* 2016;6(1):13.

35. Kang I-J, Wang L-W, Hsu T-A, Yueh A, Lee C-C, Lee Y-C, Lee C-Y, Chao Y-S, Shih S-R, Chern J-H, et al. Isatin- β -thiosemicarbazones as potent herpes simplex virus inhibitors. *Bioorg Med Chem Lett*. 2011;21(7):1948–1952.
36. Zhang HM, Dai H, Hanson PJ, Li H, Guo H, Ye X, Hemida MG, Wang L, Tong Y, Qiu Y, et al. Antiviral activity of an isatin derivative via induction of PERK^{Nrf2}-mediated suppression of cap-independent translation. *ACS Chem Biol*. 2014;9(4):1015–1024.
37. Pirrung MC, Pansare SV, Das Sarma K, Keith KA, Kern ER. Combinatorial optimization of isatin- β -thiosemicarbazones as anti-poxvirus agents. *J Med Chem*. 2005;48(8):3045–3050.
38. Selvam P, Muruges N, Chandramohan M, Sidwell RW, Wandersee MK, Smee DF. Anti-influenza virus activities of 4-[(1,2-dihydro-2-oxo-3H-indol-3-ylidene)amino]-N-(4,6-dimethyl-2-pyrimidin-2-yl)benzenesulphonamide and its derivatives. *Antivir Chem Chemother*. 2006;17(5):269–274.
39. Liu W, Zhu H-M, Niu G-J, Shi E-Z, Chen J, Sun B, Chen W-Q, Zhou H-G, Yang C. Synthesis, modification and docking studies of 5-sulfonyl isatin derivatives as SARS-CoV 3C-like protease inhibitors. *Bioorg Med Chem*. 2014;22(1):292–302.
40. Selvam P, Murgesh N, Chandramohan M, De Clercq E, Keyaerts E, Vijgen L, Maes P, Neyts J, Ranst MV. In vitro antiviral activity of some novel isatin derivatives against HCV and SARS-CoV viruses. *Indian J Pharm Sci*. 2008;70(1):91–94.
41. Chen L-R, Wang Y-C, Lin YW, Chou S-Y, Chen S-F, Liu LT, Wu Y-T, Kuo C-J, Shieh-Shung Chen T, Juang S-H. Synthesis and evaluation of isatin derivatives as effective SARS coronavirus 3CL protease inhibitors. *Bioorg Med Chem Lett*. 2005;15(12):3058–3062.
42. Zhou L, Liu Y, Zhang W, Wei P, Huang C, Pei J, Yuan Y, Lai L. Isatin compounds as noncovalent SARS coronavirus 3C-like protease inhibitors. *J Med Chem*. 2006;49(12):3440–3443.
43. Liu P, Liu H, Sun Q, Liang H, Li C, Deng X, Liu Y, Lai L. Potent inhibitors of SARS-CoV-2 3C-like protease derived from N-substituted isatin compounds. *Eur J Med Chem*. 2020;206:112702.
44. ElNaggar MH, Abdelwahab GM, Kutkat O, GabAllah M, Ali MA, El-Metwally ME, Sayed AM, Abdelmohsen UR, Khalil AT. Aurasperone A inhibits SARS CoV-2 in vitro: an integrated in vitro and in silico study. *Mar Drugs*. 2022;20(3):179.
45. Elsbaey M, Ibrahim MAA, Bar FA, Elgazar AA. Chemical constituents from coconut waste and their in-silico evaluation as potential antiviral agents against SARS-CoV-2. *S Afr J Bot*. 2021;141:278–289.
46. Elimam DM, Elgazar AA, El-Senduny FF, El-Domany RA, Badria FA, Eldehna WM. Natural inspired piperine-based ureas and amides as novel antitumor agents towards breast cancer. *J Enzyme Inhib Med Chem*. 2022;37(1):39–50.
47. Al-Sanea MM, Hamdi A, Mohamed AAB, El-Shafey HW, Moustafa M, Elgazar AA, Eldehna WM, Ur Rahman H, Parambi DGT, Elbargisy RM, et al. New benzothiazole hybrids as potential VEGFR-2 inhibitors: design, synthesis, anticancer evaluation, and in silico study. *J Enzyme Inhib Med Chem*. 2023;38(1):2166036.
48. Othman DI, Hamdi A, Tawfik SS, Elgazar AA, Mostafa AS. Identification of new benzimidazole-triazole hybrids as anti-cancer agents: multi-target recognition, in vitro and in silico studies. *J Enzyme Inhib Med Chem*. 2023;38(1):2166037.
49. Elbadawi MM, Eldehna WM, Nocentini A, Abo-Ashour MF, Elkaeed EB, Abdelgawad MA, Alharbi KS, Abdel-Aziz HA, Supuran CT, Gratterer P, et al. Identification of N-phenyl-2-(phenylsulfonyl) acetamides/propanamides as new SLC-0111 analogues: synthesis and evaluation of the carbonic anhydrase inhibitory activities. *Eur J Med Chem*. 2021;218:113360.
50. An R, Lin B, Zhao S, Cao C, Wang Y, Cheng X, Liu Y, Guo M, Xu H, Wang Y, et al. Discovery of novel artemisinin-sulfonamide hybrids as potential carbonic anhydrase IX inhibitors with improved antiproliferative activities. *Bioorg Chem*. 2020;104:104347.
51. El-Sayed HA, Moustafa AH, Masry AA, Amer AM, Mohammed SM. An efficient synthesis of 4, 6-diarylnicotinonitrile-acetamide hybrids via 1, 2, 3-triazole linker as multitarget microbial inhibitors. *J Heterocyclic Chem*. 2022;59(2):275–285.
52. Firoozpour L, Gao L, Moghimi S, Pasalar P, Davoodi J, Wang M-W, Rezaei Z, Dadgar A, Yahyavi H, Amanlou M, et al. Efficient synthesis, biological evaluation, and docking study of Isatin based derivatives as caspase inhibitors. *J Enzyme Inhib Med Chem*. 2020;35(1):1674–1684.
53. Tri NM, Thanh ND, Ha LN, Anh DTT, Toan VN, Giang NTK. Study on synthesis of some substituted N-propargyl isatins by propargylation reaction of corresponding isatins using potassium carbonate as base under ultrasound-and microwave-assisted conditions. *Chem Pap*. 2021;75(9):4793–4801.
54. Day J, Uroos M, Castledine RA, Lewis W, McKeever-Abbas B, Dowden J. Alkaloid inspired spirocyclic oxindoles from 1, 3-dipolar cycloaddition of pyridinium ylides. *Org Biomol Chem*. 2013;11(38):6502–6509.
55. Mosmann T. Rapid colorimetric assay for cellular growth and survival: application to proliferation and cytotoxicity assays. *J Immunol Methods*. 1983;65(1-2):55–63.
56. Abd-Alla HI, Kutkat O, Sweelam H-t. M, Eldehna WM, Mostafa MA, Ibrahim MT, Moatasim Y, GabAllah M, Al-Karmalawy AA. Investigating the potential anti-SARS-CoV-2 and anti-MERS-CoV activities of yellow necklacepod among three selected medicinal plants: extraction, isolation, identification, in vitro, modes of action, and molecular docking studies. *Metabolites*. 2022;12(11):1109.
57. Al-Karmalawy AA, El-Gamil DS, El-Shesheny R, Sharaky M, Alnajjar R, Kutkat O, Moatasim Y, Elagawany M, Al-Rashood ST, Binjubair FA, et al. Design and statistical optimisation of emulsomal nanoparticles for improved anti-SARS-CoV-2 activity of N-(5-nitrothiazol-2-yl)-carboxamido candidates: in vitro and in silico studies. *J Enzyme Inhib Med Chem*. 2023;38(1):2202357.
58. Elebeedy D, Elkhatib WF, Kandeil A, Ghanem A, Kutkat O, Alnajjar R, Saleh MA, Maksoud AIAE, Badawy I, Al-Karmalawy AA. Anti-SARS-CoV-2 activities of tanshinone IIA, carnolic acid, rosmarinic acid, salvianolic acid, baicalein, and glycyrrhetic acid between computational and in vitro insights. *RSC Adv*. 2021;11(47):29267–29286.
59. Abo Elmaaty A, Eldehna W, Khattab M, Kutkat O, Alnajjar R, El-Taweel A, Al-Rashood S, Abourehab M, Binjubair F, Saleh M, et al. Anticoagulants as potential SARS-CoV-2 Mpro inhibitors for COVID-19 Patients: in vitro, molecular docking, molecular dynamics, DFT, and SAR studies. *IJMS*. 2022;23(20):12235.
60. Trott O, Olson AJ. AutoDock Vina: improving the speed and accuracy of docking with a new scoring function, efficient optimization, and multithreading. *J Comput Chem*. 2010;31(2):455–461.
61. Gao S, Sylvester K, Song L, Claff T, Jing L, Woodson M, Weiße RH, Cheng Y, Schäkel L, Petry M, et al. Discovery and crystallographic studies of trisubstituted piperazine

- derivatives as non-covalent SARS-CoV-2 main protease inhibitors with high target specificity and low toxicity. *J Med Chem.* 2022;65(19):13343–13364.
62. Abraham MJ, Murtola T, Schulz R, Páll S, Smith JC, Hess B, Lindahl E. GROMACS: high performance molecular simulations through multi-level parallelism from laptops to supercomputers. *SoftwareX.* 2015;1-2:19–25.
63. Schüttelkopf AW, van Aalten DMF. PRODRG: a tool for high-throughput crystallography of protein-ligand complexes. *Acta Crystallogr D Biol Crystallogr.* 2004;60(Pt 8):1355–1363.
64. Hassab MAE, Fares M, Amin MKA-H, Al-Rashood ST, Alharbi A, Eskandrani RO, Alkahtani HM, Eldehna WM. Toward the identification of potential α -ketoamide covalent inhibitors for SARS-CoV-2 main protease: fragment-based drug design and MM-PBSA calculations. *Processes.* 2021;9(6):1004.
65. El Hassab MA, Shoun AA, Al-Rashood ST, Al-Warhi T, Eldehna WM. Identification of a new potential SARS-CoV-2 RNA-dependent RNA polymerase inhibitor via combining fragment-based drug design, docking, molecular dynamics, and MM-PBSA calculations. *Front Chem.* 2020;8:915.
66. El Hassab MA, Ibrahim TM, Al-Rashood ST, Alharbi A, Eskandrani RO, Eldehna WM. In silico identification of novel SARS-COV-2 2'-O-methyltransferase (nsp16) inhibitors: structure-based virtual screening, molecular dynamics simulation and MM-PBSA approaches. *J Enzyme Inhib Med Chem.* 2021; 36(1):727–736.
67. El Hassab MA, Ibrahim TM, Shoun AA, Al-Rashood ST, Alkahtani HM, Alharbi A, Eskandrani RO, Eldehna WM. In silico identification of potential SARS COV-2 2'-O-methyltransferase inhibitor: fragment-based screening approach and MM-PBSA calculations. *RSC Adv.* 2021; 11(26):16026–16033.